

Influence of hybrid fibrils of 2,5-bis(2-benzoxazolyl) thiophene and halloysite nanotubes on the crystallization behaviour of polypropylene

Mingxian Liu, Baochun Guo¹, Mingliang Du, Quanliang Zou and Demin Jia

Department of Polymer Materials and Engineering, South China University of Technology, Guangzhou 510640, People's Republic of China

E-mail: psbcguo@scut.edu.cn

Received 16 January 2009

Published 20 March 2009

Online at stacks.iop.org/JPhysD/42/075306

Abstract

2,5-bis(2-benzoxazolyl) thiophene (BBT) included polypropylene (PP)/halloysite nanotubes (HNTs) composites showed substantially increased mechanical properties and this was attributed to the changed crystallinity of the PP matrix by BBT (Liu *et al* 2007 *Nanotechnology* **18** 455703). This paper intends to give a detailed study on the influence of BBT hybrid fibrils on the crystallization of the PP matrix by using the observations of polarized optical microscopy (POM) and scanning electron microscopy, together with the comparisons of the activation energy of crystallization. The POM results show that PP crystals could epitaxially grow on the BBT and hybrid fibril substrates, indicating the nucleating ability of BBT. Oriented PP ribbon-like crystals with a thickness of 200 nm around BBT fibrils are observed. The formation of this unique crystal morphology is attributed to the epitaxial crystallization under the shearing orientation effect. A new transition peak well above the glass transition of PP is observed, which is attributed to the glass transition of the confined amorphous PP in the ribbon-like crystal layers around the fibrils. The fold-surface free energy of the BBT included composites is substantially decreased, suggesting facilitated crystallization in the presence of hybrid fibrils.

(Some figures in this article are in colour only in the electronic version)

1. Introduction

Isotactic polypropylene (PP), as the first representative of industrially manufactured stereoregular polymers, has been investigated extensively in the past few decades [1–4]. As a semi-crystalline polymer, its crystalline microstructural characteristics, such as crystallinity, crystal form and crystal orientation and size, have profound effects on the final properties of the polymer [5]. Introducing a nucleating agent is a simple and effective method to change the crystallization behaviour and consequently the macroscopic properties of PP. Nucleated PP always shows improved mechanical, optical and thermal properties compared with those for the neat

polymer [6–8]. Different crystal forms such as α -PP, β -PP or duplex $\alpha - \beta$ -PP and characteristic morphologies including transcrystalline, spherulite, hedrite, cylindrite and epitaxial crystallization can be developed in the nucleated PP systems depending on the nucleating agent and the crystallization condition. Unfortunately, detailed nucleating mechanisms in the nucleated polymer systems are still not very clear so far. The well-known lattice dimensional match theory can explain most of the organics nucleated polymer systems. In the theory, the matching of the unit cell parameters between the nucleating agent and the polymer matrix is considered to be responsible for the nucleation [9–13]. However, some other factors such as processing conditions and characters of the nucleating agent also play important roles in the nucleation [14, 15].

¹ Author to whom any correspondence should be addressed.

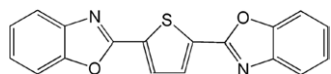
Fibres or *in situ* formed fibrils acting as heterogeneous nucleating points for polymer have been well recognized. For example, 1,2,3,4-bis-(*p*-methylbenzylidene sorbitol) (MBDS) can be organized into nanofibrils with a typical length of several micrometres and a radius about 50 nm via hydrogen bonding and/or π interaction among themselves in polymer matrix [16, 17]. These fibrils connect each other and thus form a percolated network suspended in the polymer matrix. The nucleation sites for the polymer are located on the surface of the network. The fibrillar arrangement provides a high surface-to-volume (S/V) ratio and, therefore, provides a large number of nucleation sites per unit of volume [18]. Carbon fibres and carbon nanotubes (CNTs) can also induce polymer crystallization via epitaxial growth by the solution crystallization techniques [19, 20]. CNTs can induce polymer secondary nucleation and the resulting nanohybrid shish-kebab structure possesses a unique, controllable periodicity of the kebab polymer single crystal. The inorganic whisker can also induce the shish-kebab crystals in the polyethylene composites [21].

In our previous research, we added 2,5-bis(2-benzoxazolyl) thiophene (BBT) to PP/halloysite nanotubes (HNTs) during processing for preparing composites. The formation of BBT/HNTs hybrid fibrils in the composites via electron transferring interaction with HNTs was obtained [22]. The purpose of this paper is to present a detailed investigation of the influence of hybrid fibrils on the crystallization of PP. The PP crystallization via epitaxial growth on the hybrid fibrils is elucidated.

2. Experimental

2.1. Materials

Isotactic PP, with a melt flow index of 2.84 g/10 min (after ISO-1133: 1997(E)), was purchased from Lanzhou Petrochemical Co., China. The HNTs were mined from Yichang, Hubei, China, and purified by the method introduced in [23]. The elemental composition by x-ray fluorescence (XRF) was determined as follows (wt.%): SiO₂, 58.91; Al₂O₃, 40.41; Fe₂O₃, 0.275; TiO₂, 0.071. The Brunauer–Emmett–Teller (BET) surface area of the purified HNTs was 50.4 m² g⁻¹. 2,5-bis(2-benzoxazolyl) thiophene (BBT), a common fluorescent brightener in the industry, with a melting point of 219 °C was purchased from the Guangzhou Times Chemical Factory, China, and used as received. The chemical structure of the BBT is depicted below.



2.2. Preparation of PP/HNTs/BBT composites

A two-screw extruder was used to prepare the PP/HNTs/BBT composites. The temperature setting of the extruder from the hopper to the die was 180/190/195/200/200/190 °C, and the screw speed was 100 rpm. The pelletized granules were dried for 5 h under 80 °C and then injection moulded under the temperature of 200 °C. The weight ratio of PP and HNTs is a

constant of 100/30 and the BBT content is variable in the range 0.5–10 wt% relative to PP.

2.3. Characterization

Polarized optical microscopy (POM). The morphologies of the crystallites of the composites were recorded with an Olympus BX41 polarized optical microscope with a Linkam hot stage. The extruded samples were placed between two microscopy slides, melted and pressed at 210 °C for 5 min to erase any trace of crystals. Then the samples were cooled to the desired crystallization temperatures at 10 °C min⁻¹ and the final morphology of the crystallites was recorded.

Scanning electron microscopy (SEM). The impact fractured surface of the PP/HNTs/BBT (100/30/10) composites was used to observe the morphology of the composites. For the crystallization morphology observation, the above sample was first immersed for 18 h in an acidic etchant solution (1.3 wt% KMnO₄, 32.9 wt% concentrated H₃PO₄ and 65.8 wt% H₂SO₄) to preferentially etch the amorphous PP in the spherulites and expose the remaining crystalline structure [24]. The specimens were washed with hydrogen peroxide (H₂O₂) and acetone subsequently in order to remove any residual etchant. All the specimens were coated with a very thin layer of gold before the SEM observation. The instrument used in this study was a LEO1530 VP SEM machine. The voltage of the electron beam used for SEM observation was 10 kV.

X-ray diffraction (XRD). The XRD test of the BBT, HNTs and the PP/HNTs/BBT composites was carried out at room temperature using a Rigaku D/MAX-III A diffractometer with Cu K_α radiation ($\lambda = 0.15418$ nm).

Dynamic mechanical analysis (DMA). DMA was conducted with a NETZSCH Instruments DMA 242 at an oscillation frequency and a heating rate of 1.0 Hz and 5 °C min⁻¹, respectively. The 3-point bending mode was selected and the experiments were conducted under nitrogen purging.

Differential scanning calorimetry (DSC). The non-isothermal crystallization of the samples was conducted by TA Q20. The samples were heated from ambient temperature to 210 °C at a heating rate of 40 °C min⁻¹ and held at 210 °C for 5 min to eliminate the thermal history. Then the samples were cooled to ambient temperature at a constant cooling rate of 2.5, 5, 10, 20 and 40 °C min⁻¹. The crystallization curves were recorded.

In order to apply Hoffman–Lauritzen theory, the equilibrium melting temperature (T_m^0) was first evaluated by the isothermal crystallization. To determine the equilibrium melting temperature, the isothermal crystallization of the neat PP and the composites was performed as follows: the samples were heated from ambient temperature to 210 °C at a heating rate of 40 °C min⁻¹ and then jump to the crystallization temperature of 110, 115, 120, 130 and 140 °C. The samples were crystallized at the crystallization temperature for 120 min before jumping to 40 °C. Finally, the samples were heated to 210 °C at a heating rate of 10 °C min⁻¹. The melting points under different crystallization temperatures were obtained.

According to the Hoffman–Weeks method [25], T_m^0 can be obtained by the linear extrapolation of T_m versus T_c data to intersect the line $T_m = T_c$ and the intersection point is T_m^0 .

Evaluation of Hoffman–Lauritzen parameters of non-isothermal crystallization. Hoffman–Lauritzen theory is used to evaluate physically meaningful parameters for the crystallization of the neat PP and the composites. Based on Hoffman–Lauritzen theory [26], the linear growth rate of a polymer crystal, G , depends on the temperature, T , as follows:

$$G = G_0 \exp\left(\frac{-U^*}{R(T - T_\infty)}\right) \exp\left(\frac{-K_g}{T\Delta Tf}\right), \quad (1)$$

where G_0 is the pre-exponential factor, U^* is the activation energy of the segmental jump, $\Delta T = T_m^0 - T$ is the undercooling, $f = 2T/(T_m^0 - T)$ is the correction factor, T_∞ is a hypothetical temperature at which the viscous flow ceases (usually taken 30 K below the glass transition temperature [26], T_g , in this work $T_\infty = 253.15$ for neat PP and the composites). The kinetic parameter K_g has the following form:

$$K_g = \frac{nb\sigma\sigma_c T_m^0}{\Delta h_f^0 k_B}, \quad (2)$$

where n takes the value of 4 for crystallization regimes I and III and 2 for regime II (in this work $n = 4$). b is the distance between two adjacent fold planes (for PP $b = 6.56 \times 10^{-10}$ m); σ and σ_c are the lateral and folding surface free energy ($\sigma = 8.79 \times 10^{-3}$ J m⁻² [27]), T_m^0 is the equilibrium melting temperature; Δh_f^0 is the heat of fusion per unit volume of crystal (1.34×10^8 J m⁻³) and k_B is the Boltzmann constant (1.38×10^{-23} J K⁻¹). The parameters U^* and K_g are usually determined by microscopically measuring the growth rate in a series of non-isothermal runs and substituting the measured value in the rearranged equation (1):

$$\ln G + \frac{U^*}{R(T - T_\infty)} = \ln G_0 - \frac{K_g}{T\Delta Tf}. \quad (3)$$

And in the narrow temperature region, an explicit dependence of the effective activation energy (E) on T can be derived from equation (1) as follows [28]:

$$E_\alpha(T) = -R \frac{d \ln G}{dT^{-1}} = U^* \frac{T^2}{(T - T_\infty)^2} + K_g R \frac{(T_m^0)^2 - T^2 - T_m^0 T}{\Delta T^2 T}. \quad (4)$$

E_α represents the effective activation energy when the crystallinity degree is α . Based on the nonlinear isoconversional method [29], the effective activation energy for the non-isothermal crystallization is calculated in accordance with equation (5) and the specific derivation process can be figured out by using [30, 31]:

$$\Omega(E_\alpha) = \min \left| \sum_{i=1}^n \sum_{j \neq i}^n \frac{\varphi_j \cdot I(E_\alpha, T_{\alpha,i})}{\varphi_i \cdot I(E_\alpha, T_{\alpha,j})} - n(n-1) \right|. \quad (5)$$

Here

$$I(E_\alpha, T_\alpha) = \int_{T_0}^{T_\alpha} \exp\left(\frac{-E_\alpha}{RT_\alpha}\right) dT,$$

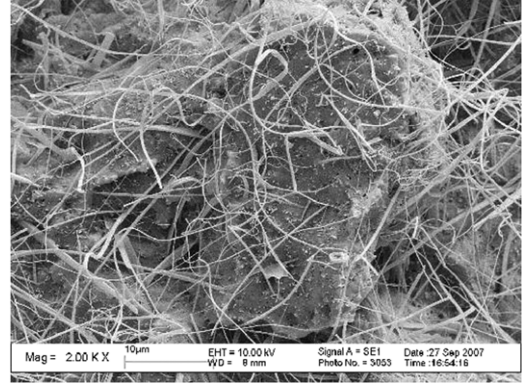


Figure 1. Typical morphology of the PP/HNTs/BBT (100/30/10) composites.

This integral is determined with the help of Doyle’s approximation:

$$I(E_\alpha, T_\alpha) \cong \frac{E_\alpha}{R} \exp\left(-5.331 - 1.052 \frac{E_\alpha}{RT_\alpha}\right). \quad (6)$$

φ stands for the cooling rate; n represents the number of cooling rates, in this study it is 5. By substituting a series of different φ_i , $T_{\alpha,i}$, ($i = 1, 2, \dots, n$) estimated at the same α on the DSC curves into equation (5), we can obtain the minimum value of E_α .

3. Results and discussion

3.1. BBT induced PP nucleation

The formation of BBT/HNTs hybrid fibrils in the PP/HNTs/BBT composites was previously reported [23]. The typical fibrous morphology is represented in figure 1. It can be seen that the fibrils which are long and continuous with a width in tens of nanometres to several micrometres are uniformly dispersed in the composites. The dispersed dense fibrils possess a large total surface area which may contain numerous sites as heterogeneous nucleation.

Many types of crystallizable organics have been reported to show the nucleating ability for polymers [32, 33]. Sorbitol-based nucleators such as 1,2,3,4-bis-dibenzylidene sorbitol (DBS), 1,2,3,4-bis-(*p*-methylbenzylidene sorbitol) (MBDS) and 1,2,3,4-bis-(*p*-methoxybenzylidene sorbitol) (DOS) were reported with a high nucleating efficiency for PP [16, 34–36]. Metal salts of substituted aromatic heterocyclic phosphate were also found to be very promising nucleators for PP. In particular, sodium 2,2’-methylene-bis-(4,6-dit-butylphenylene) phosphate (NA-11) is a powerful nucleating agent widely used in PP [37, 38]. The nucleating activity and efficiency of these organic substrates depend on their chemical composition [39–42], surface energy [43], the crystalline morphology of the nucleating surfaces [44] and the unit cell parameters of the nucleators [9–13]. BBT is also an organic crystal and can organize into fibrils in PP/HNTs/BBT composites via interaction with HNTs during processing. To elucidate the nucleating ability of

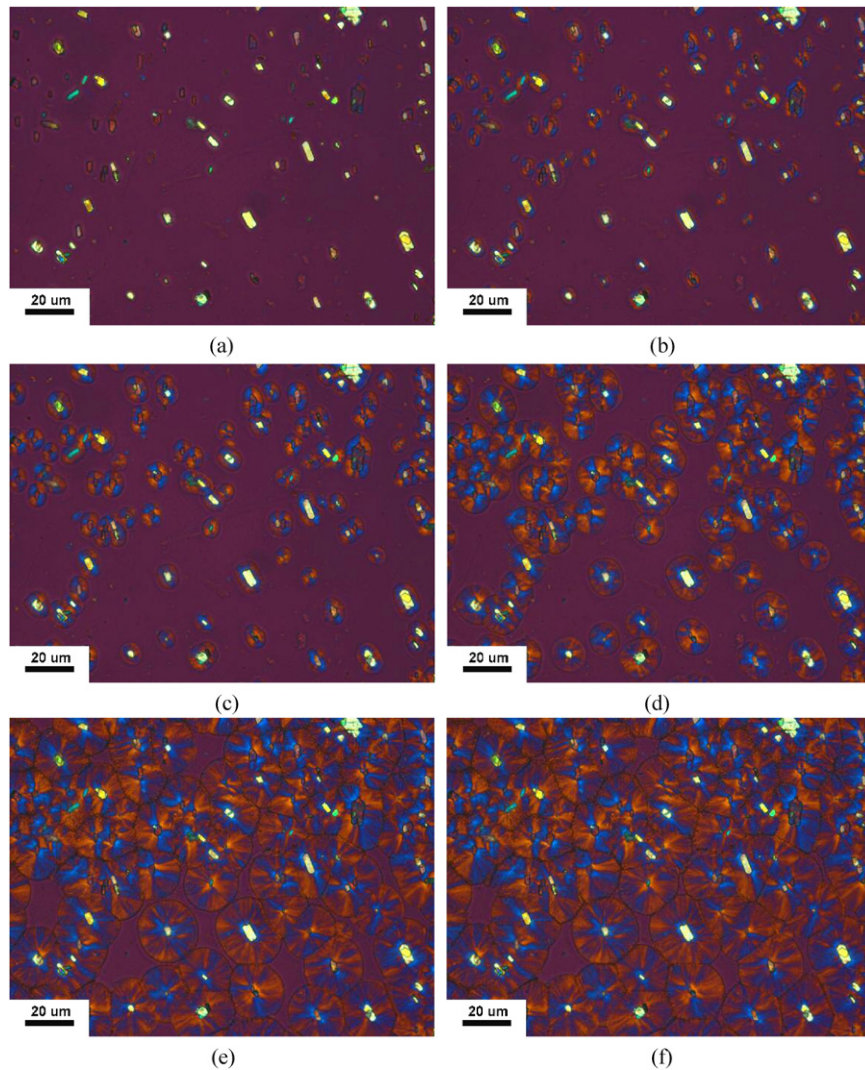


Figure 2. The evolution of the crystalline morphology during the crystallization process of the PP/BBT composites (100/10): (a) at 210 °C; (b) 120 °C × 2 min; (c) 120 °C × 4 min; (d) 120 °C × 8 min; (e) 120 °C × 20 min; (f) 120 °C × 30 min.

the fibrils, the nucleation of PP on BBT was first examined by POM observation. Figures 2(a)–(f) show the evolution of crystalline morphology during the crystallization of the PP/BBT composite. Figure 2(a) shows the photo of the sample at a temperature of 210 °C. It is clear that BBT aggregates (bright parts) are observed in the PP melt. With the decrease in temperature, the PP starts to crystallize due to heterogeneous nucleation on the BBT aggregates. PP spherulites grow from rectangular BBT aggregates until they impinge on other ones. From the POM photos, it is clear that BBT can induce PP nucleation through epitaxial growth. Apart from the spherulites nucleated by BBT, PP spherulites nucleated by themselves are also observed in the sample. The size of all these spherulites increases with crystallization time until they impinge upon each other. Hou *et al* also reported a similar nucleated PP morphology in which the nucleating agent is N,N'-dicyclohexyl-2,6-naphthalenedicarboxamide (DC26NDCA) [42]. Noticeably, the dimension of the two types of spherulites is comparable, with a diameter of about 20 μm. From the POM result, BBT

acts as a novel organics nucleator for PP with a high nucleating ability.

To further verify the ability of the nucleating ability of BBT for PP, the POM photos were taken for the ternary PP/HNTs/BBT systems and shown in figure 3. Figure 3(a) shows the POM photos of the PP/HNTs/BBT at room temperature. The coloured rod-like phase in the composite samples is the hybrid fibrils. The fibrils are uniformly dispersed in micro-scale dimension in the composites indicating the large interface between PP and the fibrils. When the sample is heated, the PP and BBT are melted and can flow freely. As no shear is applied during the observation, the hybrid fibrils re-organize into large hybrid aggregates (HNTs/BBT) and some discontinuous fibres. The final morphology of the melting sample is shown in figure 3(b). It is clear that both large hybrid aggregates in tens of micrometres and discontinuous fibres coexist in the samples. Upon crystallization, the PP crystal can epitaxially grow on the hybrid fibrils and aggregates as shown in figure 3(c) and (d). The PP crystals are clearly observed on the surface of

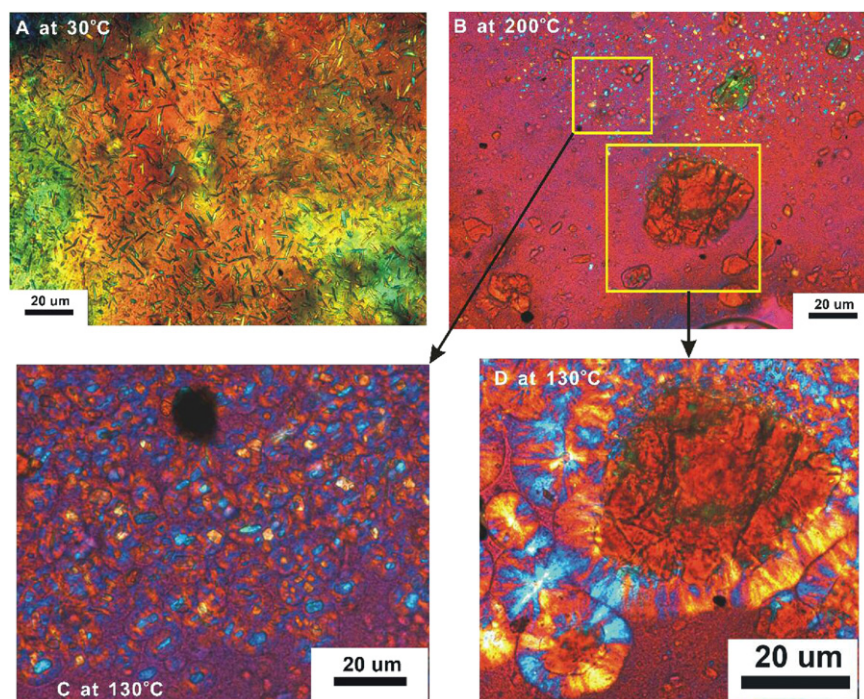


Figure 3. POM photos of the PP/HNTs/BBT (100/30/3) composites: (A) at 30 °C; (B) at 200 °C; (C) spherulites developed around the fibrils (crystallized at 130 °C × 3 min); (D) crystals developed around the hybrid aggregates (crystallized at 130 °C × 15 min).

short fibrils and hybrid aggregates. It should be emphasized that the epitaxial growth of PP crystals on the HNTs/BBT aggregates in the sample is attributed to the nucleating ability of BBT since HNT aggregates have poor nucleating ability for PP [45]. Therefore, the result further evidences the nucleating ability of BBT for PP. It should also be noted that due to the BBT in the hybrid fibrils of the ternary systems being much finer compared with BBT aggregates in the binary systems, the fibrils provide many more nuclei for the PP matrix. The largely increased nuclei for the epitaxial growth lead to smaller crystallites of PP. Actually, other organic crystals also bring about significantly decreased spherulite size by acting as the heterogeneous nucleating points for the polymers [46]. In summary, the POM experiment result for the composite gives direct evidence of the nucleating ability of BBT and BBT/HNTs hybrid fibrils.

The crystal structure of BBT in the hybrid fibrils may be changed compared with that in BBT aggregates due to the interactions between BBT and HNTs. Figure 4 shows the XRD patterns of BBT, HNTs and the composites. It can be seen that the diffraction peak at 5.43° for BBT is shifted to 5.24° for the PP/HNTs/BBT composites, indicating the slightly changed crystal structure of BBT in the hybrid fibrils. Actually, the changed diffraction is also an indication of the interactions between HNTs and BBT, which consequently promote the dispersion of BBT in the composite. The better dispersion state of BBT and HNTs provides many more nuclei for the crystal growth of the PP and consequently the crystallization behaviour and the performance of the composites may be substantially changed.

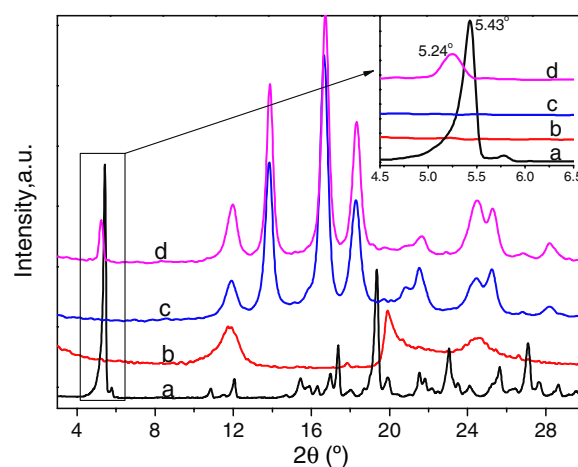


Figure 4. XRD spectrum of (a) BBT, (b) HNTs, (c) PP/HNTs(100/30) and (d) PP/HNTs/BBT(100/30/10).

3.2. Crystalline morphology of the composites containing hybrid fibrils

In order to investigate the crystalline morphology of the composites formed during processing, SEM observation for the etched PP/HNTs/BBT composites was conducted. Figure 5 shows the morphology of the etched composite sample in which the amorphous parts are essentially removed. The hybrid fibrils in the composites have also been removed as BBT can be dissolved in the acidic etchant solution. HNTs, which are inert to the etchant, are also observed. The long strip-like cavities in the photo represent the location of the fibrils in the composites as their dimension is consistent with

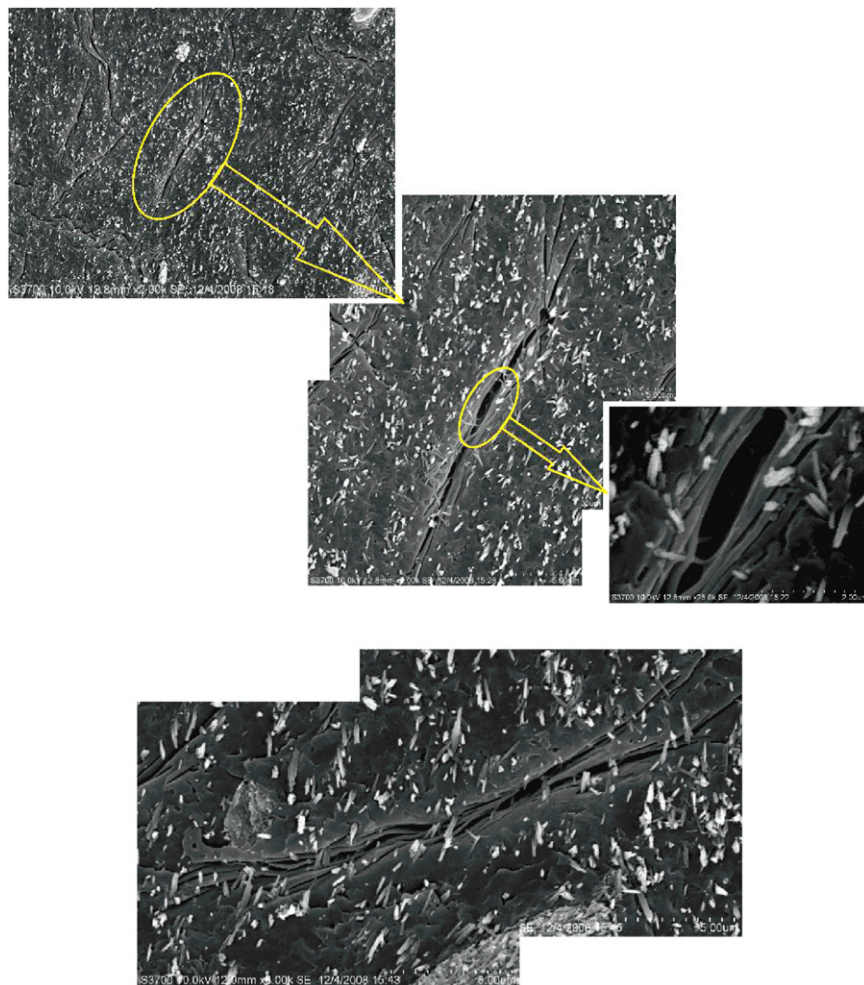


Figure 5. Crystalline morphology of the PP/HNTs/BBT (100/30/10) composite.

that of the fibrils in the unetched composites. Very clearly, ribbon-like crystals are found on the surfaces of the fibrils in the composites. The ribbon-like crystals with a thickness of about 200 nm in the crystal layer are parallel to the fibril axis which may be attributed to the strong shearing induced orientation during processing. It is noticeable that no regular spherulites are identified in the composites. Principally, two types of crystallization coexist in the system. First, the ribbon-like PP crystals epitaxially grow on the numerous nuclei on the fibrils. Second, the ‘free’ HNTs (besides those in the hybrid fibrils) may induce numerous regular spherulites. The growth of this kind of spherulite may substantially be restricted by the presence of fibrils and consequently they are invisible under SEM observation. As a result, only the unique ribbon-like crystals around hybrid fibrils are observed in the injection moulding bars.

Figure 6 shows the $\tan \delta - T$ curves determined by DMA. It can be seen that there is a main transition peak around 6 °C for all samples, which is attributed to the glass transition of the amorphous PP. Incorporating BBT in the composites, interestingly, a new small peak at a higher temperature appears in the curves. The peak temperature for the new peak is around 30 °C which is about 25 °C higher than the main peak temperature. To the best of our knowledge, this

is the first report about a new transition peak at a higher temperature for PP composites. From the above morphology result, many ribbon-like PP crystal layers are observed around the hybrid fibrils in the PP/HNTs/BBT composites in which the amorphous parts should be responsible for the unique transition. The mobility of the PP chains of the amorphous phase in the crystal layer is believed to be much confined and consequently possesses a higher glass transition temperature.

3.3. Comparison of the Hoffman–Lauritzen parameters via isoconversional method

Compared with the POM method, DSC is a quantitative method for evaluating the crystallization process. In this work, DSC tests were conducted to quantify the influence of BBT on the crystallization process for PP by computing the crystallization activation energy for different samples. Figure 7 shows the crystallization curves of the neat PP, PP/HNTs, PP/BBT and the PP/HNTs/BBT composites under different cooling rates. It can be seen that the crystallization peak temperature for all the composites with the same cooling rate is higher than that for neat PP, which indicates the nucleating effect of BBT and HNTs. Both BBT and HNTs

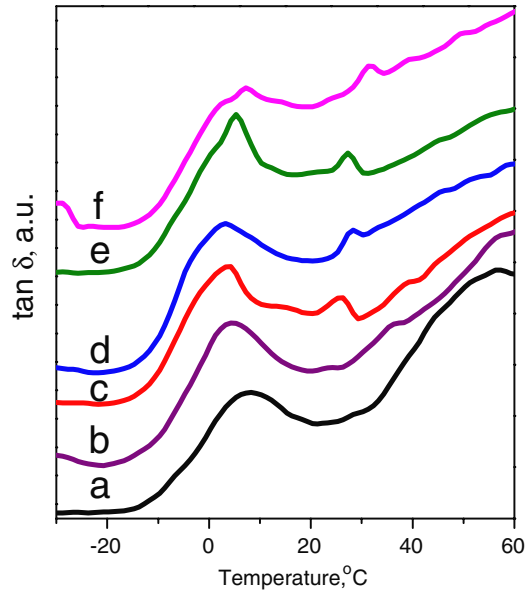


Figure 6. DMA $\tan \delta$ curves of the PP/HNTs/BBT composites (the curves are up- or down-shifted to compare): (a) neat PP; (b) PP/HNTs (100/30); (c) PP/HNTs/BBT (100/30/0.5); (d) PP/HNTs/BBT (100/30/1); (e) PP/HNTs/BBT (100/30/3); (f) PP/HNTs/BBT (100/30/10).

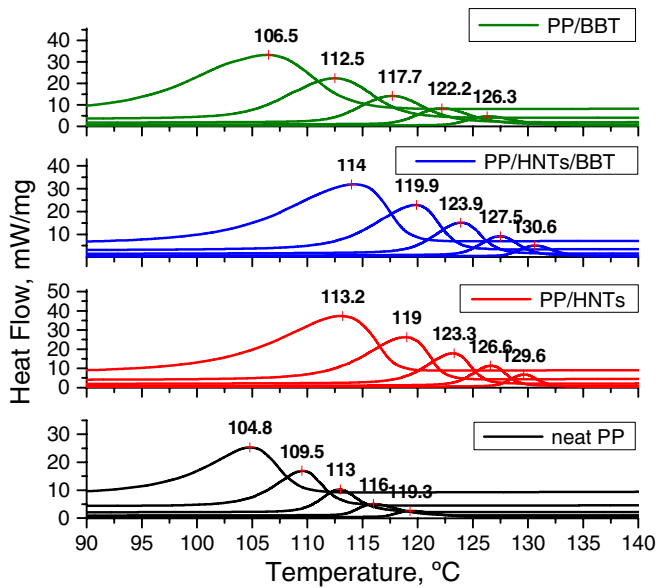


Figure 7. DSC crystallization curves of neat PP and the composites at different cooling rates of $40^\circ\text{C min}^{-1}$, $20^\circ\text{C min}^{-1}$, $10^\circ\text{C min}^{-1}$, 5°C min^{-1} and $2.5^\circ\text{C min}^{-1}$ (from left to right).

can serve as heterogeneous nucleating points for PP and this is consistent with the above POM results. It can also be seen that the composites containing hybrid fibrils show the highest crystallization temperature at all cooling rates. This further confirmed that the nucleation of PP is promoted by the formation of hybrid fibrils.

To apply Hoffman–Lauritzen theory, the T versus α curves are first established. T is the average temperature associated with the same α value for the five curves at different cooling rates. The resulting T versus α dependence for neat PP and the composites is shown in figure 8. From figure 8,

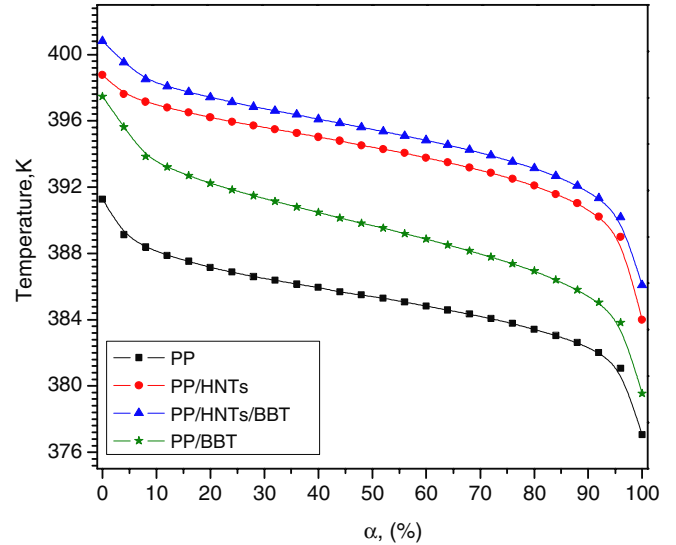


Figure 8. α - T curves of the neat PP and composites: (■) PP; (●) PP/HNTs(100/30); (▲) PP/HNTs/BBT(100/30/3); (★) PP/BBT(100/3).

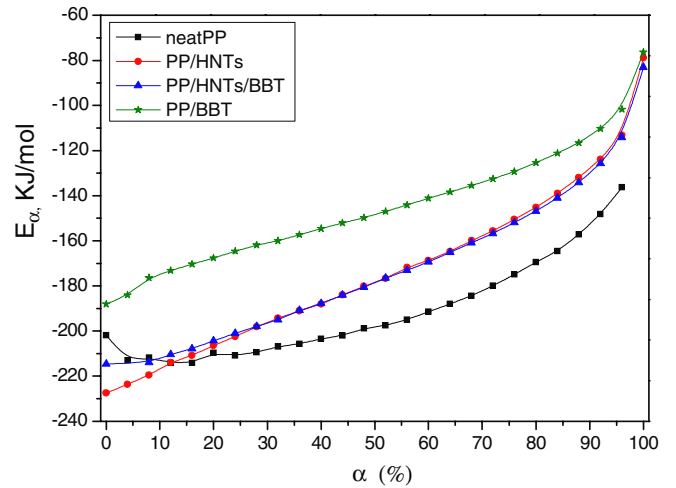


Figure 9. E_α - α curves of the neat PP and composites: (■) PP; (●) PP/HNTs(100/30); (▲) PP/HNTs/BBT(100/30/3); (★) PP/BBT(100/3).

at the same conversion, the crystallization temperatures of the composites are higher than that of PP. It can also be explained by the nucleating effect of HNTs and BBT. The T - α dependence allows us to correlate the obtained E_α values with the temperature by equation (4). Figure 9 displays the E_α dependence obtained from the DSC data on the non-isothermal crystallization of neat PP and the composites. The absolute value of E_α of neat PP and the composites decreases as α increases and at the same α the absolute value of E_α of all the composites is always lower than that of neat PP. The lower activation energy of the composites indicates facilitated crystallization for the PP matrix in the composites. This can be attributed to the nucleating ability of BBT and HNTs. The dependence of E_a on T is obtained by combining figures 8 and 9 and the results are shown in figure 10. The fitting of E_a - T curves by equation (4) with Origin7.5 software yields values of U^* and K_g and the results are summarized in table 1.

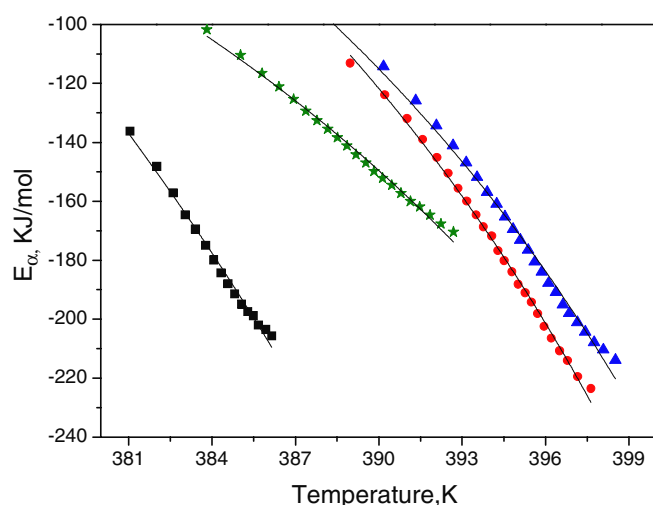


Figure 10. E_{α} - T curves of the neat PP and composites: (■) PP; (●) PP/HNTs(100/30); (▲) PP/HNTs/BBT(100/30/3); (★) PP/BBT(100/3) (the line is a fitting curve according to equation (4)).

Table 1. Kinetic data for non-isothermal crystallization of neat PP and the composites.

Samples	Neat PP	PP/HNTs (100/30)	PP/HNTs/BBT (100/30/3)	PP/BBT (100/3)
U^* (J mol^{-1})	19537.19	13839.51	11078.93	6128.79
K_g (10^5 K^2)	6.87	2.57	2.30	2.80
R^2	0.99235	0.99751	0.9952	0.99488
T_m^0 (K)	454.5	444.6	445.2	451.1
$\sigma\sigma_e$ ($\times 10^{-4} \text{ J}^2 \text{ m}^{-4}$)	10.65	4.07	3.64	4.37
σ_e (J m^{-2})	0.1212	0.0463	0.0414	0.0497

The high R^2 indicates satisfactory fitting of the data. The available K_g permits the calculation of the fold-surface free energy (σ_e) by equation (2). The values of σ_e are also listed in table 1 ($\sigma = 8.79 \times 10^{-3} \text{ J m}^{-2}$ for PP [27]). From table 1, it is noted that the values of σ_e for the composites are lower than that for neat PP. The lowest σ_e is found in the BBT containing PP/HNTs composite. The lower the values of σ_e , the less the necessary energy for the fold of the segments into the nucleus surface [47]. Therefore, the decreased values of the composite indicate that the PP chains can more readily fold into the nucleus surface. Therefore, the BBT containing system possesses the lowest folding energy of the chain into the nucleus surface. This result substantiates the facilitated crystallization process in the fibril containing composite. The decreased σ_e in the present systems is in agreement with the result of dibenzylidene sorbitol (DBS) [48], rare earth complex and N, N'-dicyclohexylterephthalamide [27] nucleated PP systems. However, an increased fold surface free energy (σ_e) is also reported in some systems, for example, the ethylene-propylene copolymer blended PP systems [49] and PP/metallocene-catalyzed polyethylene elastomer (mPE) blends [50]. The increased trend for σ_e is explained by the obstruction effect of ethylene-propylene copolymer or mPE on the surface nucleation of PP and regular folding of the molecule chains during crystallization.

4. Conclusions

The influence of the formation of BBT/HNTs hybrid fibrils on the crystallization for the PP matrix was studied. The POM results showed that PP crystals could epitaxially grow on the BBT and hybrid fibril substrates, indicating the nucleating ability of BBT. Oriented PP ribbon-like crystals with a thickness of 200 nm around the BBT fibrils were observed. The formation of this unique crystal morphology was attributed to epitaxial crystallization under the shearing orientation effect. A new transition peak well above the glass transition of PP was observed, which was attributed to the glass transition of the confined amorphous PP in the ribbon-like crystal layers around the fibrils. The fold-surface free energy of BBT included composites was substantially decreased, suggesting facilitated crystallization in the presence of hybrid fibrils.

Acknowledgments

The authors are grateful for the financial support by the National Natural Science Foundation of China with Grant numbers of 50603005 and 50873035 and the Doctorate Foundation of South China University of Technology.

References

- [1] Padden F J Jr and Keith H D 1959 *J. Appl. Phys.* **30** 1479–84
- [2] Morrow D R and Newman B A 1968 *J. Appl. Phys.* **39** 4944–50
- [3] Brückner S and Meille S V 1989 *Nature (London)* **340** 455–7
- [4] Meille S V, Brückner S and Porzio W 1990 *Macromolecules* **23** 4114–21
- [5] Jancar J 1999 Structure–property relationships in thermoplastic matrices *Mineral Fillers in Thermoplastics I (Advances in Polymer Science vol 139)* (Berlin: Springer) pp 1–65
- [6] Gurato G and Zannetti R 1980 Heterogeneous nucleation phenomena and their applications in polymer production *Chim. Indust. (Milan, Italy)* **62** 743–51
- [7] Thierry A, Straupe C, Wittmann J C and Lotz B 2006 *Macromol. Symp.* **241** 103–10
- [8] Nagasawa S, Fujimori A, Masuko T and Iguchi M 2005 *Polymer* **46** 5241–50
- [9] Wittmann J C and Lotz B 1990 *Prog. Polym. Sci.* **15** 909–48
- [10] Thierry A, Mathieu C, Straupe C, Wittmann J C and Lotz B 2001 *Macromol. Symp.* **166** 43–58
- [11] Yoshimoto S, Ueda T, Yamanaka K, Kawaguchi A, Tobita E and Haruna T 2001 *Polymer* **42** 9627–31
- [12] Alcazar D, Ruan J, Thierry A and Lotz B 2006 *Macromolecules* **39** 2832–40
- [13] Yan C, Li H H, Zhang J M, Ozaki Y, Shen D Y, Yan D D, Shi A C and Yan S K 2006 *Macromolecules* **39** 8041–8
- [14] Wang K, Chen F, Zhang Q and Fu Q 2008 *Polymer* **49** 4745–55
- [15] Li L, Li B, Hood M A and Li C Y 2008 *Polymer* doi: 10.1016/j.polymer.2008.12.031
- [16] Lipp J, Shuster M, Terry A E and Cohen Y 2006 *Langmuir* **22** 6398–402
- [17] Lipp J, Shuster M, Terry A E and Cohen Y 2008 *Polym. Eng. Sci.* **48** 705–10
- [18] Balzano L, Rastogi S and Peters G W M 2008 *Macromolecules* **41** 399–408
- [19] Li C Y, Li L Y, Cai W W, Kodjie S L and Tenneti K K 2005 *Adv. Mater.* **17** 1198–202
- [20] Li L Y, Li C Y and Ni C Y 2006 *J. Am. Chem. Soc.* **128** 1692–9

- [21] Ning N Y, Luo F, Pan B F, Zhang Q, Wang K and Fu Q 2007 *Macromolecules* **40** 8533–6
- [22] Liu M X, Guo B C, Zou Q L, Du M L and Jia D M 2008 *Nanotechnology* **19** 205709
- [23] Liu M X, Guo B C, Du M L, Cai X J and Jia D M 2007 *Nanotechnology* **18** 455703
- [24] Xu W, Martin D C and Arruda E M 2005 *Polymer* **46** 455–70
- [25] Hoffman J D and Weeks J J 1962 *J. Chem. Phys.* **37** 1723–41
- [26] Hoffman J D, Davis G T and Lauritzen J I Jr 1976 *Treatise on Solid State Chemistry* ed N B Hannay vol 3 (New York: Plenum) p 497
- [27] Xiao W C, Wu P Y and Feng J C 2008 *J. Appl. Polym. Sci.* **108** 3370–9
- [28] Vyazovkin S and Sbirrazzuoli N 2004 *Macromol. Rapid Commun.* **25** 733–8
- [29] Vyazovkin S and Dollimore D 1996 *J. Chem. Inf. Comput. Sci.* **36** 42–5
- [30] Vyazovkin S 1997 *J. Comput. Chem.* **18** 393–402
- [31] Vyazovkin S 2001 *J. Comput. Chem.* **22** 178–83
- [32] Binsbergen F L 1970 *Polymer* **11** 253–67
- [33] Libster D, Aserin A and Garti N 2007 *Polym. Adv. Technol.* **18** 685–95
- [34] Fillon B, Lotz B, Thierry A and Wittmann J C 1993 *J. Polym. Sci. B: Polym. Phys.* **31** 1395–405
- [35] Shepard T A, Delsorbo C R, Louth R M, Walborn J L, Norman D A, Harvey N G and Spontak R J 1997 *J. Polym. Sci. B: Polym. Phys.* **35** 2617–28
- [36] Kristiansen M, Werner M, Tervoort T, Smith P, Blomenhofer M and Schmidt H W 2003 *Macromolecules* **36** 5150–6
- [37] Yoshimoto S, Ueda T, Yamanaka K, Kawaguchi A, Tobita E and Haruna T 2001 *Polymer* **42** 9627–31
- [38] Zhang Y F and Xin Z 2006 *J. Appl. Polym. Sci.* **100** 4868–74
- [39] Binsbergen F L 1970 *Polymer* **11** 253–67
- [40] Beck H N and Ledbetter H D 1965 *J. Appl. Polym. Sci.* **9** 2131–42
- [41] Beck H N 1967 *J. Appl. Polym. Sci.* **11** 673–85
- [42] Hou W M, Liu G, Zhou J J, Gao X, Li Y, Li L, Zheng S, Xin Z and Zhao L Q 2006 *Colloid Polym. Sci.* **285** 11–17
- [43] Cho K W, Kim D W and Yoon S 2003 *Macromolecules* **36** 7652–60
- [44] Hobbs S Y 1971 *Nature Phys. Sci.* **234** 12
- [45] Du M L 2007 *Doctor Thesis* S China University of Technology
- [46] Karl Heinz M 1983 *Ange. Makromol. Chem.* **111** 165–77
- [47] Wang B B, Ding Z Y and Hu G S 2008 *Polym. Eng. Sci.* **48** 2354–61
- [48] Feng Y, Jin X and Hay J N 1998 *J. Appl. Polym. Sci.* **69** 2089–95
- [49] Shangguan Y G, Song Y H and Zheng Q 2007 *Polymer* **48** 4567–77
- [50] Qin J L, Zhang S Q and Li Z T 2008 *J. Appl. Polym. Sci.* **110** 2615–22